Time resolved imaging microscopy

Phosphorescence and delayed fluorescence imaging

Gerard Marriott, Robert M. Clegg, Donna J. Arndt-Jovin, and Thomas M. Jovin
Department of Molecular Biology, Max Planck Institute for Biophysical Chemistry, Postfach 2841, D-W-3400 Göttingen, Federal Republic of Germany

ABSTRACT An optical microscope capable of measuring time resolved luminescence (phosphorescence and delayed fluorescence) images has been developed. The technique employs two phase-locked mechanical choppers and a slow-scan scientific CCD camera attached to a normal fluorescence microscope. The sample is illuminated by a periodic train of light pulses and the image is recorded within a defined time interval after the end of each excitation period. The time resolution discriminates completely against light scattering, reflection, autofluorescence, and extraneous prompt fluorescence, which ordinarily decrease contrast in normal fluorescence microscopy measurements. Time resolved image microscopy produces a high contrast image and particular structures can be emphasized by displaying a new parameter, the ratio of the phosphorescence to fluorescence. Objects differing in luminescence decay rates are easily resolved. The lifetime of the long lived luminescence can be measured at each pixel of the microscope image by analyzing a series of images that differ by a variable time delay. The distribution of luminescence decay rates is displayed directly as an image. Several examples demonstrate the utility of the instrument and the complementarity it offers to conventional fluorescence microscopy.

INTRODUCTION

Fluorescence microscopy provides a sensitive means of acquiring information about the organization and dynamics of complex cellular structures (for a historical review see Kasten, 1989). In the last decade, technological advances in image detectors, computer hardware, and lasers have been extensively employed in fluorescence microscopy, leading to dramatic improvements in quantitative image acquisition and analysis (for reviews see Kohen and Hirschberg, 1989; Arndt-Jovin et al., 1985; Jovin and Arndt-Jovin, 1989; Wang and Taylor, 1989; Aikens et al., 1989). The design and use of new luminescent probes have also proceeded at a rapid pace (Tsien, 1989; Haugland, 1989). To date, the intensity, the excitation and emission spectral dispersion, and the relative polarization of steady-state prompt fluorescence have been used to form images and to distinguish particular molecular complexes or the local environment of labeled species in microscopic preparations. Fig. 1 *c* presents a simple energy level diagram demonstrating the approximate spectroscopic transition rates to and from selected energy states of a molecule. The diversity in the values of the rates is apparent from this illustration; the rates of long lived emission are generally orders of magnitude apart from prompt emission. Although delayed luminescence from chromophores, i.e., phosphorescence and delayed fluorescence, provides significant spectroscopic and molecular information (Parker, 1968), only sporadic applications of these spectroscopic techniques for measuring microscope images from biological material have been made (Harvey and Chase, 1942; Vialli, 1964; Polyakov et al., 1966; Zotikov & Polyakov, 1975, 1977; Zotikov, 1982). An instrument to measure the position-dependent decay time of either prompt or delayed luminescence in a microscope image has not yet been reported.

The contrast within an image and the discrimination between different fluorophores or probe environments can be improved by exploiting the temporal domain of emission. Time resolved measurements of intensity and anisotropy have been used in solution studies to resolve the emission from a mixture of several simultaneously fluorescing species into separate spectroscopic components (O'Haver and Parks, 1974; Gratton and Jameson, 1985). Time resolved delayed luminescence spectroscopy has been applied to solutions and cell suspensions in order to determine the rotational freedom of molecular complexes in cell membranes (Garland and Moore, 1979; Austin et al., 1979) and to measure the excited state kinetics of dye interactions with DNA (Geacintov et al., 1981; Corin et al., 1985). The extended time range (microseconds to seconds) is suitable for observing macromolecular dynamics that are too slow to be studied with prompt fluorescence methods. Delayed luminescence also provides a sensitive assay for the determination of oxygen concentration in solution (Vanderkooi et al., 1987; Englander et al., 1987). The measurement of time resolved luminescence images in a microscope makes it possible to directly determine dynamic spectroscopic properties within localized regions of an image. The image measurement supplements the correspond-

0006-3495/91/12/1374/14 $2.00

ing solution and suspension studies, and the time resolution complements the steady-state information available from images recorded in a conventional fluorescence microscope.

We present a simple time resolved delayed luminescence microscope capable of recording images of very weak long lived luminescence from organic chromophores used as stains for biological material. The luminescence time decay can be determined simultaneously at every pixel of the image. Several applications demonstrating the utility of the technique are presented. We illustrate the method by reporting distributions of the delayed luminescence intensities and lifetimes of acridine dyes in 3T3 cells and bound to polytene chromosome preparations. N-bridged heterocyclic dyes such as acridine orange (AO), proflavine, and phosphine are known to emit from the excited singlet and triplet states in anoxic fluid solutions (Kautsky et al., 1935; Zanker, 1952; Parker, 1968). The binding of AO to DNA in solution has been extensively studied with various spectroscopic techniques (Rigler, 1966; Steiner, et al., 1970; Darzynkiewicz, 1979), including time resolved phosphorescence spectroscopy in solution (Geacintov et al., 1981; Corin and Jovin, 1986). We have presented preliminary descriptions of the time resolved microscope in previous publications (Jovin, et al., 1989; Jovin, et al., 1990; Jovin and Arndt-Jovin, 1989).

MATERIALS AND METHODS

Reagents

Acridine orange and proflavine were purchased from Merck and phosphine from BDH Chemical Company (Poole, Dorset, UK). Glucose oxidase and catalase were purchased from Sigma Chemical Company (St. Louis, MO). All other reagents were of the highest purity available.

Staining with noncovalent dyes and sample preparation

Subconfluent 3T3 cells were grown on cover slips and labeled with AO, phosphine, and proflavine as follows. After removing the growth medium, the cells were washed with PBS and bathed in DMEM and 10% fetal calf serum containing freshly prepared dye at the specified concentrations at 37°C for 30 min. Subsequently, the cover slips were washed with PBS containing 0.87 mM $CaCl_2$ and 0.5 mM $MgCl_2$, and then mounted in the same buffer containing the same concentration of dye, 0.05 mg/ml glucose oxidase, 0.035 mg/ml catalase, and 50 mM glucose. For some experiments with high concentrations of AO (>5 μM) the dye was excluded from the mounting and washing media. The edges of the cover slips were sealed to the slide with nail varnish and incubated at 37°C for 30 min. Because the long lived triplet state is particularly sensitive to dynamic quenching processes, primarily collision with molecular oxygen, anoxic solutions greatly enhance the probability of triplet emission in organic molecules. Removal of oxygen from the mounting buffer can be achieved enzymatically with the coupled glucose oxidase-catalase system described above (Englander et al., 1987). We have also found efficient deoxygenation in the absence of catalase. Although depleted of oxygen, the living cells remain viable for several hours at temperatures between 4–37°C, presumably by using anaerobic pathways for survival. Fixed cells or acetic acid squashes of salivary gland chromosomes were either mounted directly in PBS containing the appropriate dye concentration and the deoxygenation system described above, or were stained for 10 min with excess dye, washed 30 min in PBS, and mounted in deoxygenation buffer without additional dye.

Instrumentation

An epi-illumination Zeiss Universal Microscope (Carl Zeiss, Inc., Oberkocken, Germany) (Fig. 1 *a*, *top*) has been modified by adding an emission filter wheel and incorporating two phase-locked rotating light choppers (HMS 221; Ithaco, Ithaca, NY). The relative phase of the rotating blades is adjusted and phase-locked to each other by means of the internal phase-lock-loop in the driving electronics, either by using one chopper as master, or by triggering both choppers with individually phase adjusted outputs of an external pulse generator (model DG53; Stanford Research Instruments, Palo Alto, CA). One light chopper intercepts the exciting light beam external to the microscope and the second is positioned in the path of the image optics in the microscope. The emission chopper is placed directly in front of the CCD camera close to the image plane. A slit of variable width can be placed directly before the chopping blade to limit the extent of the image in the direction of the blade movement, thereby increasing the time resolution. We have modified the emission chopper module such that it is easily inserted as a single unit in the microscope. The instrument can operate in both prompt fluorescence and delayed luminescence modes. The duty cycle of the excitation chopper, that is, the fraction of time the exciting light impinges on the sample, is variable. For the measurements in this report it was 10–20%, whereas the emission chopper usually had a 50% open duty cycle. The measurements shown in this report used a Spectra-Physics, Inc. 2025 argon ion laser (Mountain View, CA) as a light source, although a mercury arc lamp has also been successfully applied.

To achieve maximum flexibility in the adjustment of the relative phase difference between the excitation light pulse and the emission light chopper, and as a convenient way to vary the period of the excitation pulse, we have also incorporated an acousto-optic modulator (AOM; Coherent, Palo Alto, CA) into the laser excitation beam. The AOM is triggered from the emission chopper electronics, and its timing is electronically adjusted so that the AOM is actuated only during the time that the excitation chopper is open to the light beam. The light beam corresponding to the first order diffraction emerging from the AOM is selected with an iris and directed into the fiber optics. The AOM pulse length is chosen to be less than the excitation chopper open time. Because discrimination against prompt fluorescence is critical in order to measure a reliable delayed luminescence image, the excitation chopper is retained in the light path to eliminate stray laser light originating in the AOM. If even a small amount of excitation light leaks through the excitation light path during the dark period of the phosphorescence measurement, a "ghost" fluorescence image appears. This can be digitally subtracted if a corresponding background image is recorded, but it is desirable to minimize this interference.

The measured quantum yield of a triplet probe $\phi_T = k_p/(k_p + k_c + k_q)$ is established by the natural radiative emission rate k_p from the triplet state, the collisional quenching rate k_q of the triplet state, and the nonradiative decay rate due to internal conversion k_c from the triplet state to the ground singlet state (see Fig. 1 *c*, *bottom*). The quantum yield of delayed luminescence for organic dyes is often less than the prompt fluorescence quantum yield by at least a factor of 100 in fluid deoxygenated solutions at room temperature (Parker, 1968;

Carmichael and Hug, 1989). Consequently, imaging of delayed luminescence of organic dyes requires sensitive photon detection. We used a Photometrics (Tucson, AZ) series 200 camera system incorporating: (*a*) a mechanical shutter; (*b*) a thermoelectrically cooled CSF-Thomson 7882(1)A CCD sensor with a Metachrome II down converter coating to boost the blue sensitivity, and a 576 × 384 array of 23 × 23 μm square pixels, each with a full well capacity of 3.5×10^5 electrons and a dark current of 8 electrons s^{-1}; (*c*) a readout noise of 6 electrons; (*d*) a 14-bit 50 kHz double correlated analogue to digital converter; and (*e*) a camera controller and image storage and display unit with communication to a central DEC MicroVax II processing system to record and subsequently analyze the digital images. The advantages of digital imaging microscopy, and, in particular, acquisition with this type of camera, have been described elsewhere (Aikins et al., 1989; Hiraoka et al., 1987; Jovin and Arndt-Jovin, 1989).

It is important to emphasize that the temporal resolution of the delayed luminescence measurement, and consequently the delayed luminescence lifetimes, are independent of the CCD readout time, the CCD sensitivity, and the response time of the electronic recording system. The temporal resolution of the system is determined by (*a*) the rate of light modulation (the repetition rate of the light choppers, $1/T'$ of Fig. 1*b*) and (*b*) how soon the observation can begin after the excitation light has been blocked (Δt of Fig. 1 *b*), as explained in the Appendix. The CCD camera accumulates the light energy passing

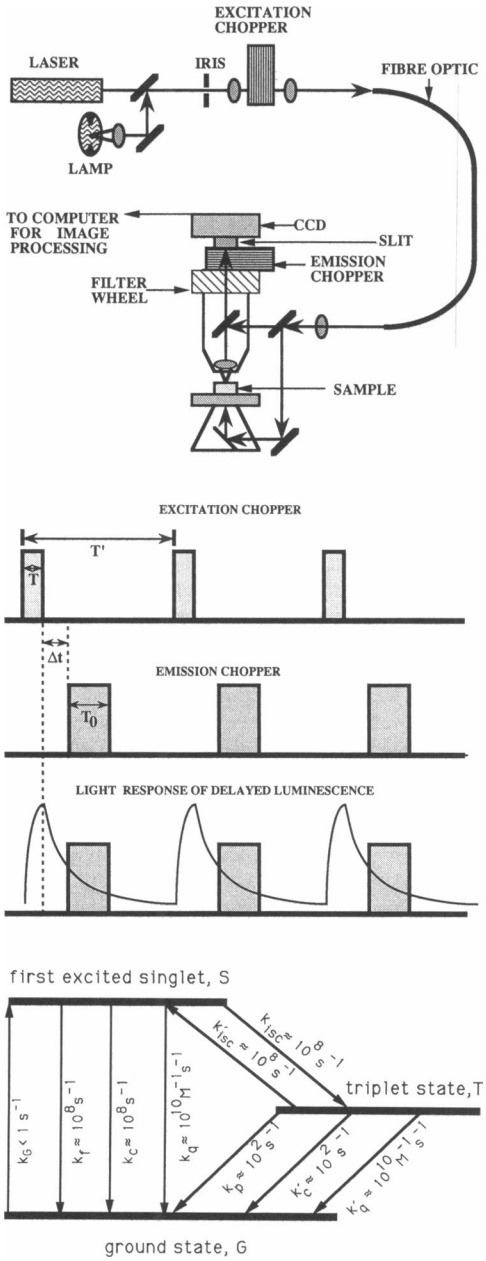

FIGURE 1

FIGURE 1 (*a*) (*top*) Schematic of the phosphorescence microscope showing the optical components. The excitation source can be a laser or arc lamp. The excitation light is focused onto the rotating excitation chopper blade so that the on-off transit time of the excitation pulse is a minimum. It is convenient to lead the light into the microscope through a quartz fiber optic. The usual mode of operation uses epiillumination, reflecting the excitation light onto the sample with dichroic mirrors. The emission passes through light filters (narrow and pass dielectric or high wavelength cutoff filters) which can easily be selected with a filter wheel. The emission chopper and slit assembly are placed as close to the camera image plane as possible. Both choppers rotate at the same frequency and are phase locked as described in the text and Fig. 1 *b*. The image is recorded and integrated on the CCD camera and then transferred to the computer for further processing with a DEC MicroVax II computer. Preprocessing of the image is also possible on the Photometrics 200 camera controller unit. (*b*) Timing diagram defining the open chopper times. The repetition period of the experiment, T', can vary from 170 μs to an arbitrarily long time. The excitation chopper pases excitation light for a period T. After the falling edge of the excitation period, which defines the zero time point, the beginning of the emission observation is delayed by ΔT, and the emission chopper passes the delayed emission to the CCD camera for a period of T_0. All of these times can be varied; ΔT is electronically continuously variable, and this is the usual method to determine the lifetime at every pixel of the image, although other modes can be used (see text). The bottom diagram shows the time dependence of the delayed luminescence intensity buildup and decay within the sample, and the shaded rectangle indicates the time over which this signal is integrated on the CCD camera. (*c*) (*bottom*) Energy level diagram showing the approximate rates from one electronic state of the molecule to another electronic state. The higher vibrational sublevels for each electronic state are not shown. The vertical arrows indicate rates of conversion between two singlet states (electrons with opposed spins), and the diagonal arrows indicate conversion rates between a singlet (electrons with opposed spins) and a triplet state (electrons with parallel spins), respectively. The rate constants are: k_G = the excitation rate due to the impinging light (G → S, see Appendix, the rate given is for 1 W cm^{-2} of 500 nm light), k_f = the radiative rate of prompt fluorescence (S → G), k_c = the radiationless rate of internal conversion (S → G), k_q = the radiationless rate of external quenching (S → G, this is a biomolecular rate constant), k_{isc} = the radiationless rate of intersystem crossing (S → T), k_p = the radiative rate of phosphorescence (T → G), k'_c = the radiationless rate of internal conversion (T → G), k'_q = the radiationless rate of external quenching (T → G, this is a biomolecular rate constant), k'_{isc} = the radiationless rate of intersystem crossing (T → S). The rates given are approximate rates often reported, and can vary by a few orders of magnitude. The actual values for the rates, except for the radiative processes, are often temperature and environmental dependent.

through the emission light chopper during its open period T_o, collected over the total recorded train of excitation cycles (Fig. 1 *b*). Because the measurement is not limited by dynamic restrictions of the recording equipment, it is not necessary to perform a deconvolution during the data analysis of a series of time delay measurements. The fitting process is done independently of, and subsequent to, the measurement, yielding the intensity, and the time decay constant, at every pixel of the image. The independence of the temporal resolution of the measurement from the time response of the CCD camera is most clearly appreciated by reference to Fig. 1 *b*.

Digital image data analysis and spectroscopic measurements

The decay parameters for the time resolved delayed luminescence images are determined as discussed in the Appendix. The image data manipulation and graphics display are performed with the software package, TCL-Image from The Delft Center for Image Processing, (Delft, Holland) augmented with other programs written in C and Fortran.

Absorption measurements were taken on a Uvikon 820 (Kontron Analytical, Zurich, CH, Switzerland) spectrophotometer. All steady-state fluorescence experiments were made with an SLM 8000S (Urbana, IL) instrument. Prompt fluorescence lifetime measurements were carried out with the method of phase and modulation on an instrument that has recently been described (Piston et al., 1989). Phosphorescence spectra and solution lifetime measurements have been made with an instrument constructed in this laboratory, which functions analogously to the microscope measurement described in Fig. 2 *b* (*bottom*), also with a pair of rotating choppers.

RESULTS

Calibration, ultimate sensitivity, and temporal resolution of the delayed luminescence microscope

The phase relation of the choppers for generating time resolved delayed luminescence images in the microscope is shown in Fig. 1 *b* (*middle*). A crucial performance factor of the microscope is the complete rejection of both excitation light and prompt fluorescence emission when the two choppers are operated in an out-of-phase mode, that is, no temporal overlap between the open periods of the excitation and emission chopper blades. A rigorous test for this condition is a prolonged integration during the dark period of the repetitive excitation sequence on the CCD camera of a strongly fluorescing or highly scattering object. We have determined this out-of-phase interference in two ways. First, we have measured the image of aerated fixed polytene chromosomes brilliantly stained with coumarin or propidium iodide, and found the rejection of the prompt fluorescence image to be better than 1 part in 10^7. This is the limit of our present selectivity. Second, only diffuse background phosphorescence is seen by passing 100 mW of 514 nm laser light through the emission path of the microscope for 50 s in the absence of emission filters, with the two choppers operating in the out-of-phase mode. This background is probably phosphorescence from the objective lens and other optical components. It is subtractable and is observed only during prolonged sample excitation with very high light intensities.

We use the rejection of prompt fluorescence to determine the absolute time delay between the two chopper blades. The zero phase condition ($\Delta t = 0$) occurs when the trailing edge of the excitation light pulse and the leading edge of the emission blade sector are coincident. The repetition rate ($1/T'$), and duration of the excitation (T) and emission (T_0) periods are known, and the zero phase position between the two choppers can be determined from intensity measurements of a highly fluorescent sample as a function of the phase delay angle between the blades.

The time between the end of the excitation period and the beginning of the delayed luminescence image recording is the operational dead time of our measurements. This delay includes the time for the excitation (or emission) chopper to travel across the excitation beam (or emission beam). At a 1 kHz repetition rate we can approach to within 50 μs of the end of the excitation pulse without interference from diffuse scattering or an image originating from the prompt fluorescence. The diffuse background is due to photons from the intense prompt fluorescence and light scattering that pass around the chopper blade before the emission chopper is geometrically open to the slit. This background can be recorded and subsequently subtracted from the sample signal yielding the corrected phosphorescence image. The imposition of a slit close to the emission chopper blade reduces this background. Despite the time resolution limit of the simple mechanical choppers compared with an acousto optical modulator, this method offers practical advantages, such as absolute darkness during the dark period and the use of any light source, such as an arc lamp, which affords a continuous light spectrum with a wide wavelength range, high stability, convenience, and low cost.

Prompt fluorescence and steady-state delayed luminescence imaging of AO in living and fixed cells

Solution spectroscopic analysis of AO bound to RNA and DNA. Earlier measurements of steady-state AO emission in solution at room temperature (Rigler, 1966) suggested the existence of at least two AO molecular states that differ in their emission characteristics: (*a*) green fluorescence is emitted from AO molecules in the monomer state. The quantum yield depends upon the particular complex that AO forms. (*b*) Red fluorescence is emitted from the aggregated state of the dye, for

instance, AO that is aggregated on the surface of a polyelectrolyte or on a negatively charged membrane surface. This explanation for the spectral attributes has recently been disputed. Darzynkiewicz and Kapuscinski (1990) contend that aggregated AO emits no red prompt fluorescence, but only red phosphorescence; they base their conjecture on spectroscopic studies of AO at −175°C (Zanker, 1952). We have determined the fluorescence and phosphorescence lifetimes of AO and its complexes in solution at room temperature, both free and bound to DNA and RNA. Details of this will be presented separately, but the main points important for this study are summarized here.

A strong green prompt fluorescence is observed under conditions that are suitable for monomer AO species, such as intercalation complexes with double-stranded DNA or RNA, AO distributed sparsely throughout membranes and detergents, or alone in aqueous or alcoholic solution. The lifetime of the green emission at 520 nm is always found to be between 1.7–1.9 ns, whether the dye is bound to DNA or RNA, complexed to SDS, or free in solution. The lifetime of the green emission remains constant whether red emission is simultaneously observed or not. Red prompt fluorescence appears whenever conditions are favorable for dye aggregation on polyanion surfaces, especially at higher dye concentrations (>10 μM) and higher dye/polyanion ratios. The ratio of red to green prompt fluorescence depends strongly upon the concentration of the dye and the ratio of dye/polyanion. The number of the decay modes and the values of the lifetimes depend on the type of polyanion and the extent of aggregation; the lifetimes vary between 5 and 20 ns. With a mixture of 16S and 23S RNA, the longer lifetime of 16–18 ns is dominant for emission greater than 630 nm.

Phosphorescence of AO is normally not observed in room temperature solutions because the phosphorescence quantum yield of nonquenched AO is low relative to the brighter red fluorescence, and the presence of oxygen in aqueous solutions is sufficient to quench dynamically and completely the delayed luminescence. In anoxic solutions the apparent phosphorescence quantum yield of AO bound to 16S and 23S RNA is lower, and the lifetime is shorter, than for AO bound to the same concentration of DNA corresponding to the fraction of total base pairs that are double-stranded in 16S and 23S RNA. The majority of the phosphorescence seen in RNA solutions is apparently due to binding of AO to the double-stranded secondary structure. The red phosphorescence from AO (lifetime ~1 ms) is observed even (and always) from solutions that exhibit no, or extremely little, red prompt fluorescence. The phosphorescence from natural DNA and RNA solutions is observed only in the red. However, for poly[d(A-br^{5}U)] and for poly[d(G-br^{5}C)] green delayed fluorescence is also observed; this is also the case for stained cell suspensions (3T3 cells) even in the absence of brominated nucleotides. Our results in solution and in the microscope are in accordance with earlier reports in the literature (Steiner et al., 1970; Geacintov et al., 1981); however, our data are contrary to the conjectures of a recent review on AO that the entire red emission of oxygenated AO-nucleic acid solutions at room temperature is phosphorescence (Darzynkiewicz and Kapuscinski, 1990).

Living cells. AO is a weak base and readily permeates living mammalian cells becoming localized in a number of intracellular structures. The metachromic prompt fluorescence image of AO in living cells is strongly dependent upon the concentration of the free dye in the bathing medium, the length of incubation, the temperature, and the metabolic state of the cell (Robbins & Marcus, 1963; Robbins et al., 1964). At high concentrations of AO in the bathing solution (5–100 μM) and after an incubation for 30 min at 37°C, the red prompt fluorescence becomes predominantly localized in the lysozomes (data not shown). This observation is in agreement with that of Zelenin (1966), whereas we found in addition that these same organelles exhibit virtually no delayed emission (e.g., see Fig. 2 *B*, for lower AO concentrations). We noticed that continued excitation of these highly labeled AO cells results in the lysis of the lysozomes within minutes, even in the absence of oxygen, with a concomitant decrease in the prompt fluorescence in the lysozomes and an increase in the prompt red fluorescence staining of the nuclear region. A similar phenomenon has been observed in the presence of O_2 by Delic et al. (1991). Conversely, the phosphorescence images ($\lambda > 590$ nm) of living anaerobic 3T3 cells labeled with these high concentrations of AO show staining predominantly in the nucleus localized similarly to the prompt green fluorescence. The phosphorescence from these cells is attenuated between 100–10,000-fold compared with the prompt fluorescence signal, depending upon which structures are viewed. As expected, no delayed luminescence signal from AO is observed in the presence of oxygen, irrespective of the dye concentration. The presence of oxygen strongly promotes dye photolysis, whereas only a small degree of photobleaching (~5% with 100 s of high intensity excitation) is detected under anoxic conditions. We find a wide range of values for the ratio of the quantum yields of the delayed luminescence to the fluorescence of AO in these cells.

At lower AO concentrations (500 nM to 2 μM) the cellular organelles become differentially labeled as seen in the fluorescence and phosphorescence images (Fig. 2, *A* and *B*, *top* and *bottom*). In addition, the red prompt

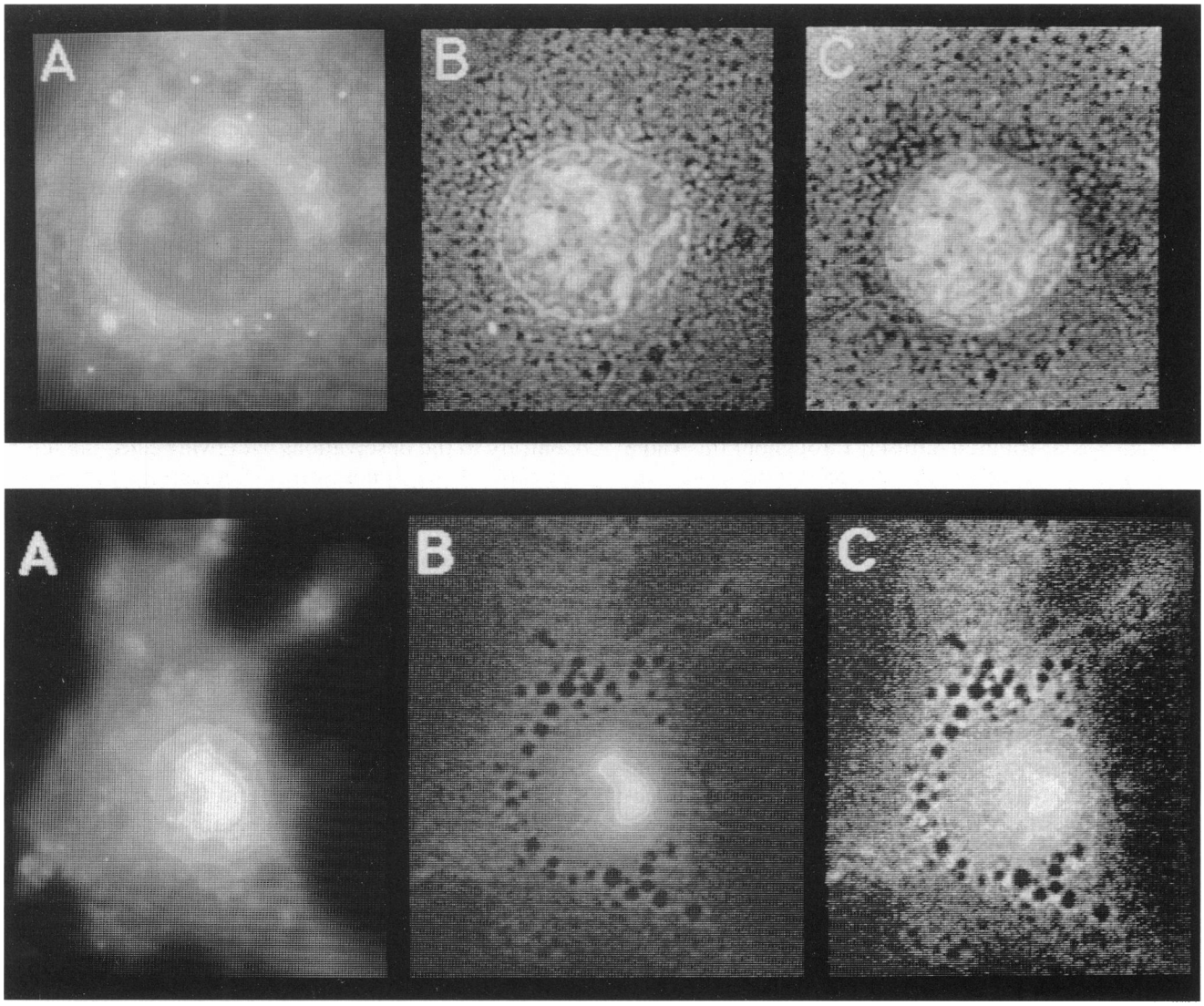

FIGURE 2 Prompt fluorescence and delayed emission images of living 3T3 cells which have been bathed in a solution with [AO] = 0.5 μM (*top*) and 1.0 μM (*bottom*). The exciting light is 488 nm. Oxygen has been removed by glucose oxidase/catalase as described in the text. The top panel shows images for [AO] = 0.5 μM: (*A*) red fluorescence, $\lambda_{em} > 650$ nm; (*B*) red phosphorescence, $\lambda_{em} > 650$ nm; and (*C*) the ratio image of phosphorescence/fluorescence (*B*/*A*). The bottom panel shows images for [AO] = 1.0 μM: (*A*) red fluorescence, $\lambda_{em} > 650$ nm; (*B*) red phosphorescence, $\lambda_{em} > 650$ nm; and (*C*) the ratio image of phosphorescence/fluorescence (*B*/*A*).

fluorescence is no longer dominated by the lysozomes and the nucleus becomes one of the prominent features of the image. It has been reported that green prompt fluorescence is derived from AO intercalated in DNA, and red prompt fluorescence is emitted from AO stacked onto a polyelectrolyte structure, including RNA (Rigler, 1966; Steiner et al., 1970). However, at these low AO concentrations the distributions of the green and red prompt fluorescence within the nucleus cannot be clearly distinguished, even in the nucleoli. Because the phosphorescence is generally quite similar to the green prompt fluorescence in live cells, we conclude that the creation of the triplet state is favored by intercalated or unstacked dye molecules. This is consistent with the lack of phosphorescence in the lysozomes and other cytoplasmic organelles where the dye is highly concentrated. These conclusions are in agreement with a detailed study by Steiner et al. (1970), who suggested that only the unstacked form of the dye bound to deoxy- and ribopolynucleotides has red phosphorescence, whereas the aggregated state of AO fluoresces red. Our solution studies (see above) at room temperature support these

conclusions. Our results also clearly indicate that aggregated AO molecules in living cells do not phosphoresce, but do fluoresce brightly in the red; this is especially evident in the ratio image (phosphorescence/fluorescence) (panel *C*, Fig. 2), where the areas of high fluorescence and little phosphorescence appear as black holes outside the nucleus.

The phosphorescence of AO staining at low dye concentrations shows much more detail in the nucleus than at higher dye concentrations. The nuclear membrane and the chromatin around the nucleoli as well as other structured chromatin are clearly defined in the phosphorescence image in the presence of 0.5 μM AO (Fig. 2 *B*, *top*). The red prompt fluorescence is strongest in the perinuclear region, particularly in the lysozomes, although it is distributed diffusely throughout the whole cell (Fig. 2 *A*). In contrast to the phosphorescence image, no particular nuclear structures except the nucleoli can be distinguished in the red prompt fluorescence.

The ratio image (phosphorescence/fluorescence) suggests that the red phosphorescence in the nucleus reflects the DNA concentration distribution that would be expected if phosphorescence arises from dye intercalated in the DNA. Thus, we seen an image of the aggregated heterochromatin distributed nonuniformly throughout the nucleus. In addition, the complete lack of phosphorescence in the lysozomes produces a high contrast ratio image in which the number and dimensions of the lysozomes are particularly evident (panel *C*, Fig. 2).

The increase in the quantum yield of the red fluorescence signal from the lysozomes has been discussed in the literature (Robbins et al., 1964) and has been attributed to two causes: (*a*) the lysozomes sequester AO that at high concentrations forms an aggregated dye complex which fluoresces in the red, and (*b*) the low pH present in the lysozomes is sufficient to increase the quantum yield of the red fluorescence. Whatever the reason for the high red fluorescence quantum yield of AO in the lysozomes, AO does not phosphoresce significantly at room temperature in this molecular environment.

The above examples clearly show the increase in the detail and contrast of microscope images, and the additional information that may be realized with a time resolved instrument.

Fixed cells. The major intensity from all the luminescent species in fixed 3T3 cells stained with high concentrations of AO is localized in the nucleus (Fig. 3). Contrary to the observations with living cells, the intensity ratio of (phosphorescence/fluorescence) in the nucleoli is very low (Fig. 3 *C*), corresponding to an increased red fluorescence that is perhaps due to the removal of some proteins during the fixing procedure leading to an increased dye binding to the RNA in the stacked state. In addition, a bright structure (crescent) adjacent to the nucleus that is often not obvious in either of the original images (Fig. 3, *A* and *B*, or in the green fluorescence image) appears in the ratio image. Based upon the arguments of the preceding paragraph, we presume that the appearance of the crescent is due to nonaggregated dye molecules and that single-stranded RNA molecules are not present at this location, because both of these conditions would lead to a lower level of phosphorescence relative to red fluorescence. There is no strong green fluorescence from this region of the image, indicating the absence of DNA. Presently we can only conjecture about the nature of this structure.

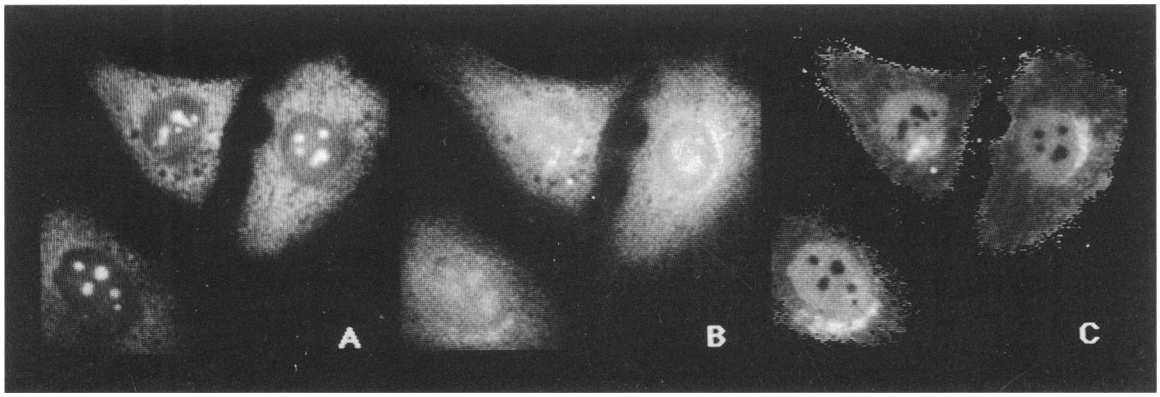

FIGURE 3 Prompt fluorescence and phosphorescence of 3T3 cells which have been fixed in 80% ethanol for 15 min at −20°C, washed, and then bathed in buffer with 50 μM AO. Oxygen is removed as in Fig. 2. See text for details. (*A*) red fluorescence, $\lambda_{em} > 650$ nm; (*B*) red phosphorescence, $\lambda_{em} > 650$ nm; and (*C*) the ratio image of phosphorescence/fluorescence (*B*/*A*).

Indirect evidence suggests that it may be a clustered form of the Golgi elements (Lipsky and Pagano, 1985; Ho et al., 1989) that is particularly visible with AO phosphorescence staining after alcohol fixation. Here again the delayed luminescence image resolves structures not apparent in the prompt fluorescence images derived with spectral discrimination alone.

Steady-state imaging of proflavin and phosphine in fixed 3T3 cells

Prompt fluorescence and phosphorescence images of phosphine and proflavine stained fixed 3T3 cells show primarily nuclear staining. We have not observed any distinct differentiation between the prompt fluorescence and phosphorescence images for either of these dyes in any cellular structure, a point highlighted by the uniformity of the phosphorescence/prompt fluorescence ratio images (data not shown). The phosphorescence of both dyes is located predominantly in the nucleus, with little cytoplasmic luminescence.

Time resolved delayed luminescence imaging of AO on polytene chromosomes and 3T3 cells

Several methods to determine delayed luminescence lifetimes from an image are possible with our instrument (see Fig. 1 *B*). (*a*) The time delay Δt between the choppers is varied at a constant modulation frequency; (*b*) the frequency of modulation $1/T'$ is changed keeping a constant phase difference between the choppers, i.e., $\Delta t / T' =$ constant; or (*c*) the width of the excitation pulse T is varied at a constant repetition frequency and a constant time delay from the end of the excitation pulse to the beginning of the observation, i.e., $\Delta t =$ constant, and the increase in phosphorescence signal is measured as the excitation pulse is lengthened. These methods have been previously established from solution measurements (Delorme & Perrin, 1929; Parker, 1968). A more complete analytical expression relating the lifetime to the frequency-dependent measured intensity, including the transient contributions if the measurement time is not long enough for the steady-state solution to be valid, is presented in the Appendix, Eqs. A1 and A6. The different methods of measuring the lifetimes, as well as the effect of the probability of triplet excitation with high light intensity, are easily derived from these equations.

The phase, or time, delay mode of operation (Fig. 1 *B*) was introduced by Delorme and Perrin (1929) for use with a Becquerel phosphoroscope (Becquerel, 1868). The delayed luminescence intensity at each pixel in the image depends upon the delay of the observation window after the excitation pulse, Δt of Fig. 1 *B*, as shown in the Appendix, Eq. A6. The delayed luminescence intensity from AO bound to a polytene chromosome decays as a function of the delay of the observation time as shown in the sequence of images in Fig. 4, panels 0–9. Photobleaching of AO during the measurement was less than 5%, as determined by repeating the initial image immediately after completing the phase shift series. Delayed luminescence lifetimes can be determined from the images on a pixel-by-pixel basis assuming a single exponential decay (see Appendix). The mean τ value was 1 ms for this image series with a coefficient of variation of 12%. Fig. 5 shows the decay analysis of another chromosome series. The range of phosphorescence lifetimes found in each pixel is tight as seen in the τ image in which the mean is 0.88 ms with a coefficient of variation of 10%. The differences between the original images (Fig. 5, panels *B* and *b*) and their reconstructed images (*C* and *c*) calculated from the fitted decay parameters at each pixel (panel τ) show very low residuals (*D* and *d*). Although the assumption of a single exponential phosphorescence decay at every pixel may appear too simplistic given the complex nature of the system, it does provide a reasonable account of the mean decay rate of the dye in every pixel. The constancy of the phosphorescence lifetime, which is independent of the position of the dye on the chromosome, is consistent with the proposal that the phosphorescent form of the dye is intercalated as a monomer form between nucleotide bases. This is analogous to the green fluorescing dye species, which is known to be intercalated and removed from solvent variations and perturbations. Similar decay analyses were made on fixed cells stained with AO for which lifetimes of 0.8–1.2 ms were found.

As an alternative to the above time delay mode we have determined the delayed luminescence lifetime at every pixel from the intensities in a series of images, varying the chopping frequency at a constant phase relation between two choppers. The lifetimes analysis in this mode of data acquisition and analysis agrees with the results of the time delay mode (data not shown).

Recovery of concealed objects with time resolved imaging

Many fluorescence microscope measurements are plagued by unwanted background fluorescence or scattering. That a phosphorescence image can remove such interfering signals is demonstrated in Fig. 6. The intense overall fluorescence in the prompt fluorescence image (Fig. 6 *A*) obscures the chromosomal DNA luminescence. Because the intercalated dye displays phosphorescence emission, whereas the aggregated dye on tissue

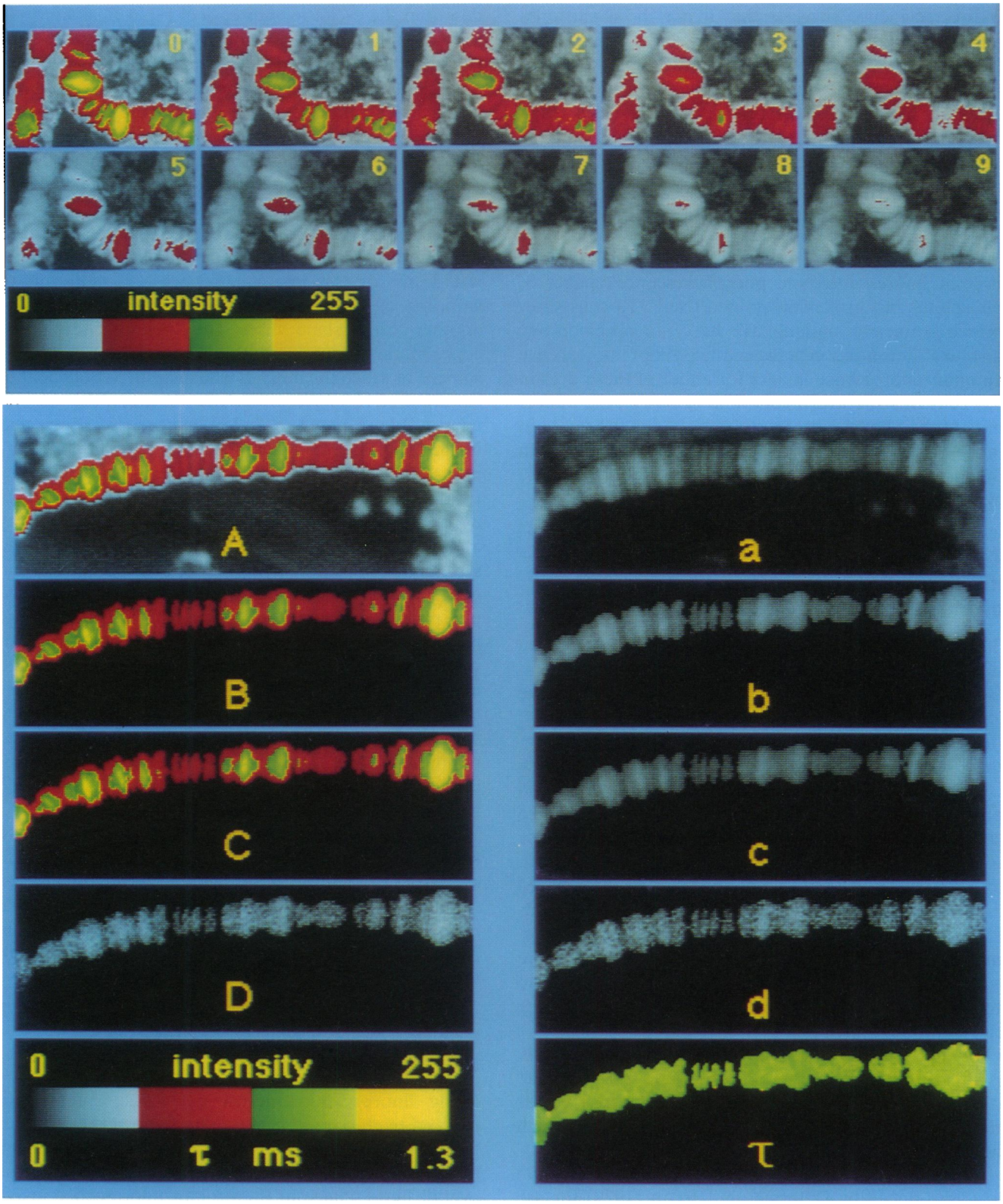

FIGURES 4 and 5

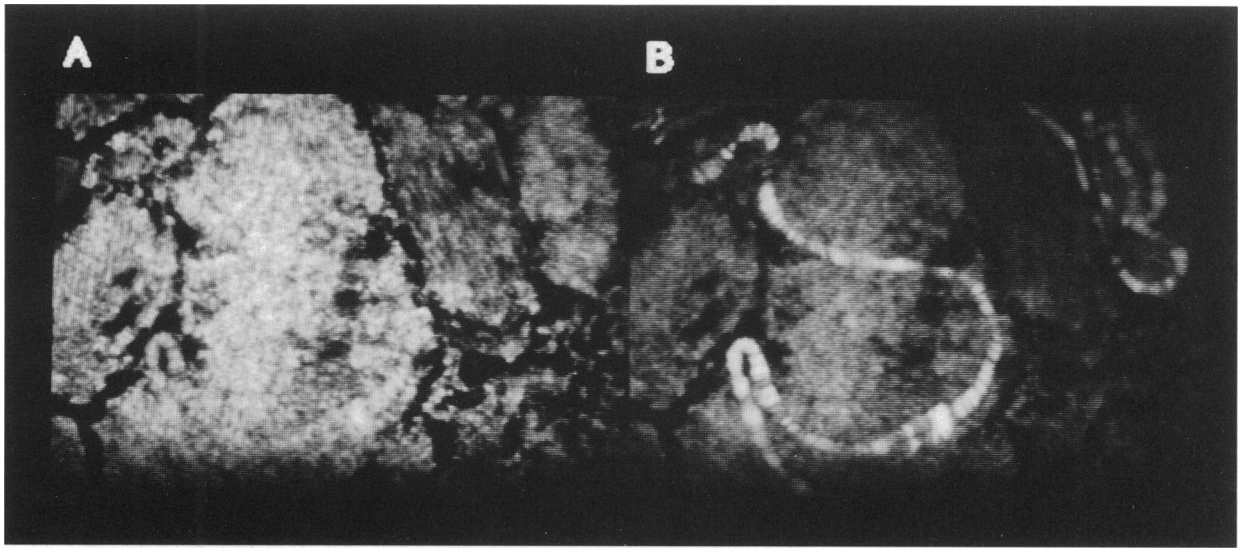

FIGURE 6 Prompt and delayed red luminescence (> 590 nm) of an AO stained polytene chromosome that is covered with tissue. The excitation wavelength is 488 nm and the sample has been prepared similarly to that of Fig. 4. In the prompt fluorescence image (*A*) the chromosome is obscured by fluorescence emitted from dye bound to the overlying tissue. The chromosome is clearly visible in the phosphorescence image (*B*), which is seen only after a time delay, because the dye bound to the tissue emits less delayed luminescence. See text.

and membranous material does not, a detailed and sharp image of a chromosome is revealed in the phosphorescence image (Fig. 6 *B*). The phosphorescence banding patterns of the chromosome in this image are very similar to that seen with DNA specific fluorescence dyes.

DISCUSSION

By exploiting the temporal attributes of spontaneous light emission, long lived luminescence provides a useful and convenient imaging technique in cellular biology and complements prompt-fluorescence microscopy. Light scattering, reflection, autofluorescence, and extraneous prompt fluorescence are all problems associated with normal fluorescence microscopy, which can decrease the sensitivity and contrast of specific signals. Time resolved spectroscopic measurements eliminate these interferences by observing the luminescence emission only after the excitation light beam has been obstructed. With the instrumentation described here, the delayed luminescence of the sample can be recorded at times as short as 50 μs after the excitation pulse ends; thus, all the advantages and applications of delayed luminescence spectroscopy can be realized. The low level of delayed emission from organic phosphores that we detect is not

FIGURE 4 (*top*) Time delayed image sequence. The phase of the emission chopper of each consecutive image has been delayed by 200 μs from the corresponding previous frame (*1–9*). The delayed emission decay constant at every pixel throughout the image is determined from the series of images as described in the text. Acid squashes of polytene chromosomes from *Drosophila melanogaster* were prepared as described in Materials and Methods. The samples were stained with a 5 μM solution of AO. Glucose oxidase/catalase and 50 mM glucose were then added and the cover slip sealed with nail polish. The color scale for intensities from 0 to 255 grey levels is shown below the series. The mean τ value is 1 ms with a standard deviation of 10% (see cover plate).

FIGURE 5 (*bottom*) A time delay determination of phosphorescence decay lifetimes in each pixel of an image of an AO stained *Drosophila melanogaster* polytene chromosome. The delay between consecutive images of the original data is 200 μs (the actual series of data is not shown here but the conditions are similar to Fig. 4). The panels are: (*A*) image at the beginning (minimum) delay time: (*a*) image at the minimum delay time plus 2 msc; (*B* and *b*) identical to the images of *A* and *a* except that the undesired portion of the image has been removed (masked); (*C* and *c*) the simulated images of *B* and *b* using the parameters of the fit to reconstruct the amplitude at each pixel; (*D* and *d*) the difference images created by multiplying the absolute residuals by 8, that is, $[(B)-(C)] \times 8$ or $[(b)-(c)] \times 8$, respectively; and (τ) the image formed from the lifetimes of the phosphorescence at every pixel. The color scale, in the bottom left panel, extends from 0 to 255 for the intensities of the images and from 0 to 1.25 ms for the amplitudes of τ; the mean τ value is 0.88 ms with a coefficient of deviation of 10%. See the text for details.

observable in a normal fluorescence microscope even in the absence of oxygen due to the intense prompt fluorescence, which is several orders of magnitude larger. The phosphorescence to prompt fluorescence image ratio, Eq. A7, a new parameter, can be computed and displayed, and in some cases structures can be discerned which are not distinct in either the fluorescence or the phosphorescence image (Figs. 2 *C* and 3 *C*). This quantity is directly proportional to the ratio of quantum yields of delayed to prompt luminescence, Eq. A7. As is apparent from this equation, the experimental conditions can be varied to optimize the value of this ratio. By adjusting the parameters of the light choppers, certain delayed luminescence lifetimes can be accentuated in the image. The long lived triplet state is very sensitive to external quenchers (such as oxygen) and the decay time of delayed luminescence can be used as a reporter of the spatial distribution of these perturbing molecular species. The phosphorescence/fluorescence ratio image is also useful in this respect, particularly because the value of this ratio is independent of the concentration of the luminophores, and depends only upon the molecular spectroscopic parameters.

The luminescence decay rate is an absolute photophysical parameter of the emission that can be used to define and compare luminescence systems and experimental conditions. The wide spectrum of delayed emission decay times assists in the discrimination of simultaneous emission from multiple probes. Instead of resolving a mean lifetime or a sum of delayed luminescence lifetimes from 10^5–10^6 cells in suspension (Johnson and Garland, 1981; Jovin and Vaz, 1989), or from a larger partial area of a cellular image (Zotikov and Polyakov, 1977), 10^5–10^6 pixel lifetimes can be resolved in the image. These decay times can then be displayed as a lifetime image, thus introducing a new dimension, a kinetic map (Fig. 5τ), into microscopy. Because the long decay times of delayed luminescence coincide with the time scales of many molecular and cellular dynamic processes in biological systems, the display of phosphorescence anisotropy decay rates, which can be calculated from the stored images of linearly polarized images, will produce similar rotational mobility distributions.

We can summarize the advantages and future applications of time resolved image microscopy as follows. *(a) Increased probe repertoire.* Multiparameter imaging of cellular structures provides a powerful technique to investigate synergistic or coupled phenomena resulting from external stimuli or cell metabolism (DeBiasio et al., 1987). With steady-state fluorescence microscope measurements, the maximum number of spectral components that can be resolved is limited by the extent of the absorption and the emission spectral overlap of each species. The addition of the temporal dimension to spectrally resolved luminescence microscopy provides the means to overcome this limitation. The number of resolvable components can be doubled by simply imaging both the steady-state fluorescence and delayed luminescence of selected luminophores in a microscope, even at the same wavelength. Figs. 2 and 3 represent examples of this particular imaging technique where we have obtained differential images of AO emission in 3T3 cells based only on the probability of singlet versus triplet emission decay processes.

(b) Increased contrast and sensitivity. The inherent fluorescence of living cells limits the sensitivity of steady-state fluorescence microscopy. Although detectors are sensitive to single photon detection, extrinsic probes applied to biological cells are normally not detected in the range of 10^3–10^4 fluorophore molecules due to autofluorescence. Time resolved imaging with long lived luminescence avoids this problem, and by using high quantum yield phosphors, transition-state and heavy metal-ion organic chelates, and lanthanides (Hemillä et al., 1984; Vanderkooi et al., 1987; Beverloo et al., 1990), the sensitivity could reach the level presently detectable by fluorescence microscopy.

(c) Time resolved environmentally sensitive imaging. Translational and rotational movements of macromolecular assemblies occur in a time range comparable to the lifetimes of delayed luminescence of many probes. Thus, an image of the delayed luminescence lifetimes can directly report spatial information about the dynamics of molecules and their immediate environment. The decay of emission anisotropy, which reports upon rotational dynamics, can be calculated from the lifetime measurements of certain polarized components. This direct information in an image may relate directly to the size and shape of the molecules or the viscosity of the molecular environment.

(d) Determination of intracellular quenching concentrations. The intensities and the decay times in delayed luminescence are sensitive to much lower concentrations of quencher molecules, implying that we often must eliminate universal quenchers, such as oxygen, from the bathing solutions; conversely, this circumstance provides an excellent analytical technique to determine the concentration of such species in tissue (Rumsey et al., 1988) and within single cells. A time resolved microscope can provide this information directly throughout the image. The spatial distribution of the lifetime in the specimen reflects the interaction of quenchers or energy acceptors with the triplet probe and to the movement of this probe in its environment during the excited-state lifetime.

APPENDIX

Mathematical formulae for the time dependent measurement of phosphorescence

Decay of the triplet state: basic expressions and definitions. A simple representation of a spectroscopic excitation-emission process considering only three molecular electronic species, the ground (G), first excited singlet (S), and triplet (T) states, is defined by the following schematic,

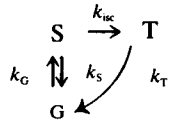

where k_G is the excitation rate constant (light intensity × absorption probability) with units of s^{-1},

$$k_G = (5.02 \cdot 10^{12}) \cdot \lambda \cdot \sigma \cdot I_0$$
$$k_G = (1.92 \cdot 10^{-8}) \cdot \lambda \cdot \epsilon \cdot I_0,$$

where the units are: I_0, the impinging radiant illuminance of the excitation light in $W \cdot cm^{-2}$, λ in nanometers, σ (the molecular cross section, $\sigma = 2303 \cdot \epsilon / N_A$) in cm^2, and ϵ in liter $\cdot$ mole$^{-1} \cdot$ cm^{-1}. As an example, if $\epsilon = 10^5$ liter $\cdot$ mole$^{-1} \cdot$ cm^{-1} ($\sigma = 3.82 \cdot 10^{-16}$ cm^2), $I_0 = 1$ watt $\cdot$ cm^{-2}, and $\lambda = 500$ nm, we have $k_G = 0.96\ s^{-1}$. k_S is the total rate away from the S state, including all nonradiative deactivation paths, except the intersystem crossing rate, k_{isc}; k_T is the total rate away from the triplet state, T. The rate (units of s^{-1}) at which the triplet state is excited, for constant rate of excitation, k_G, is

$$R_T = \frac{k_G \cdot k_{isc}}{(k_S + k_{isc})}.$$

For this kinetic scheme, the time decay of the triplet state concentration as a function of the time Δt after the end of the excitation period (see Fig. 1), Triplet (Δt), for our experimental conditions can be shown to be,

$$\text{Triplet}(\Delta t) = \frac{\left(\frac{G_0 \cdot R_T}{(R_T + k_T)}\right) \cdot (1 - e^{-N(R_T T + k_T T')}) \cdot (1 - e^{-(R_T + k_T)T})}{(1 - e^{-(R_T T + k_T T')})} \cdot e^{-k_T \Delta t}. \quad \text{(A1)}$$

T, T', and Δt are defined in Fig. 1 *b*. The time Δt is the elapsed time after the Nth excitation pulse has stopped. N is the number of excitation periods after which the signal is observed. $G_0 = [G] + [S] + [T]$ (i.e., the total concentration of the spectroscopically active molecular species). The radiative rates (s^{-1}) from the S and T states are k_f and k_p, respectively. The fluorescence quantum yield, Φ_f, (number of fluorescence photons emitted/number of photons absorbed) is

$$\Phi_f = \frac{k_f}{(k_S + k_{isc})}.$$

Likewise, the usual quantum yield of phosphorescence, Φ_p, (number of phosphorescence photons emitted/number photons absorbed), is

$$\Phi_p = \left(\frac{k_p}{k_T}\right) \cdot \left(\frac{k_{isc}}{(k_S + k_{isc})}\right).$$

We define a quantum yield of triplet decay, Φ_T, (number of phosphorescence photons emitted/number of triplet molecules created) to be

$$\Phi_T = \frac{k_p}{k_T}.$$

The two delayed luminescence quantum yields are related by

$$\Phi_p = \left(\frac{k_{isc}}{(k_S + k_{isc})}\right) \cdot \Phi_T.$$

The time dependence of the excitation light is expressed as $I_0(t) = I_0 \cdot f(t)$, where I_0 is the intensity of the uninterrupted impinging light, and $f(t)$ is a time varying function with a maximum value of one (Fig. 1 *b*).

Eq. A1 is similar to an expression given by Parker (1968), but the term

$$(1 - e^{-N(R_T T + k_T T')})$$

is new. This term represents the buildup of the triplet state to the steady-state value, and must be taken into account if the data acquisition is begun before the steady-state is attained. If the total time of excitation is long before the start of the data acquisition, that is $N(R_T T + k_T T') \gg 1$, this term equals 1. If we are observing and averaging only over times during which the steady-state concentrations are obtained, the exponential term involving N drops out, and the total equation becomes:

$$\text{Triplet}(\Delta t) = \frac{\left(\frac{G_0 \cdot R_T}{(R_T + k_T)}\right) \cdot (1 - e^{-(R_T + k_T)T})}{(1 - e^{-(R_T T + k_T T')})} \cdot e^{-k_T \Delta t}. \quad \text{(A2)}$$

We have also explicitly retained the triplet excitation rate term (R_T) in the equations, because for high laser irradiance in the microscope the value of k_G can be close to the value of k_T.

Steady-state concentrations and intensities with constant illumination. The steady-state concentration of the triplet state, Triplet$_{ss}$, with a constant light illumination and therefore a constant rate of excitation, k_G, is

$$\text{Triplet}_{SS} = \left(\frac{G_0 \cdot R_T}{(R_T + k_T)}\right) = \frac{G_0 \cdot \left(\frac{k_{isc} \cdot k_G}{k_S + k_{isc}}\right)}{\left(\frac{k_{isc} \cdot k_G}{[k_S + k_{isc}]} + k_T\right)}. \quad \text{(A3)}$$

Triplet$_{SS}$ of Eq. A3 is the total concentration of the luminescent molecule multiplied by the ratio of the rate of excitation to the triplet state divided by the sum of the rate of excitation and emission from the triplet state. In general the light intensity is not high enough to deplete the ground state, so that

$$\text{Triplet}_{SS} = \left(\frac{G_0 \cdot R_T}{(R_T + k_T)}\right) \cong \left(\frac{G_0 \cdot k_{isc} \cdot k_G}{k_T \cdot (k_S + k_{isc})}\right) \quad \text{(A4)}$$

$k_p \cdot$ Triplet$_{SS}$ is the intensity of the steady-state phosphorescence signal with a constant excitation rate of k_G. The steady-state fluorescence intensity for the same conditions is $k_f \cdot G_0 \cdot (k_G/k_G + k_S + k_{isc}) \cong k_f \cdot G_0 \cdot (k_G/k_S + k_{isc})$; k_f is the radiative rate from the first excited singlet.

Therefore the ratio of the steady-state phosphorescence (phos) intensity to the steady-state fluorescence (fluor) intensity is

$$\text{Ratio}_{SS}\left(\frac{\text{phos}}{\text{fluor}}\right) = k_p \cdot \text{Triplet}_{SS} / \left(\frac{G_0 \cdot k_G k_f}{(k_S + k_{isc})}\right) = \left(\frac{k_{isc}}{(k_S + k_{isc})}\right) \cdot \left(\frac{k_p / k_T}{k_f / (k_S + k_{isc})}\right)$$

or, using the above definitions

$$\text{Ratio}_{SS}\left(\frac{\text{phos}}{\text{fluor}}\right) = \left(\frac{k_{isc}}{(k_S + k_{isc})}\right) \cdot \frac{\Phi_T}{\Phi_f} = \frac{\Phi_p}{\Phi_f} = \frac{k_{isc} \cdot k_p}{k_f \cdot k_T}. \quad \text{(A5)}$$

Similar expressions are indicated by Parker (1968). The measured values of the quantum yields are only proportional to the true values of the quantum yields, Φ_p and Φ_f. If the spectra of the delayed luminescence and the prompt fluorescence are identical then the ratio, Φ_p/Φ_f, will equal the measured ratio of intensities. This is usually not even approximately true if the delayed luminescence is phosphorescence, because then the emission originates from different excited states. In this case the ratio must be corrected for the areas under the emission spectral curves.

The measured time-dependent delayed luminescence signal and the ratio of delayed to prompt luminescence. The expression for the actual measured phosphorescence signal in our experiment must take into account the intermittent excitation light and the fact that the phosphorescence intensity is integrated for a time period T_0, from Δt to $\Delta t + T_0$. The measured phosphorescence signal is found by multiplying Eq. A2 by k_p and integrating from Δt to $\Delta t + T_0$.

Integrated phosphorescence intensity

$$= k_p \cdot \int_{\Delta t}^{\Delta t + T_0} \text{Triplet}(\Delta t) \cdot d(\Delta t)$$

$$= \left(\frac{k_p}{k_T}\right) \cdot \text{Triplet}_{SS} \cdot (1 - e^{-k_T T_0}) \cdot \left(\frac{1 - e^{-(R_T + k_T)T}}{1 - e^{-(R_T T + k_T T')}}\right) \cdot e^{-k_T \Delta t}$$

$$= \left(\frac{\Phi_p \cdot G_0 \cdot k_G}{k_T}\right) \cdot (1 - e^{-k_T T_0}) \cdot \left(\frac{1 - e^{-(R_T + k_T)}}{1 - e^{-(R_T T + k_T T')}}\right) \cdot e^{-k_T \Delta t}, \quad \text{(A6)}$$

where Triplet_{SS} is given by Eq. A4. The integrated fluorescence signal for one cycle of excitation is $G_0 \cdot k_G k_f / (k_S + k_{isc}) \cdot T$, where T here refers to the time defined in Fig. 1 *b*. The ratio of the measured integrated phosphorescence and fluorescence signals is,

$$\left(\frac{\text{phos}}{\text{fluor}}\right)_{\text{integrated intensity}} = \left(\frac{k_p}{k_T}\right) \cdot \text{Triplet}_{SS} \cdot (1 - e^{-k_T T_0}) \cdot \left(\frac{1 - e^{-(R_T + k_T)T}}{1 - e^{-(R_T T + k_T T')}}\right) \cdot e^{-k_T \Delta t}$$

$$= \left(\frac{\Phi_p}{\Phi_f}\right) \cdot \frac{(1 - e^{-k_T T_0})}{(k_T \cdot T)} \cdot \left(\frac{1 - e^{-(R_T + k_T)T}}{1 - e^{-(R_T T + k_T T')}}\right) \cdot e^{-k_T \Delta t}. \quad \text{(A7)}$$

This last expression assumes that the timing conditions of Fig. 1 *b* pertain to both the phosphorescence and fluorescence measurements. It is also assumed that the prompt fluorescence is collected during the time of excitation, with $T < T_0$, and that both signals are collected for the same number of excitation cycles. Usually the latter condition does not hold, and a simple multiplicative correction is needed to take this into account. In all experiments reported in this paper the light intensity is small enough so that $R_T \cong 0$, which simplifies Eq. A7 further. It is straightforward to derive all special modes and approximations of the experiments from this general equation.

Fitting the time delayed images to an exponential function, pixel by pixel. The time dependence of the delayed luminescence at every pixel i is modeled by a single exponential decay, $A_i \exp(-t/\tau_i) + B_i$, where τ_i is the decay time of luminescence. A_i, τ_i, and B_i are the parameters to be determined. To reduce the computational time as much as possible, a region of interest in the image is selected by a simple thresholding operation, typically yielding 10^4–10^5 pixels. The data are fit by a nonlinear least square analysis, avoiding iteration cycles by directly solving the normal equations corresponding to the above model. A polynomial is derived in terms of the variable $u = \exp(-\Delta t/\tau)$, where Δt is the constant time interval between consecutive images, the total number of which defines the order of the polynomial. Note that for the kth time point, $\exp(-t_k/\tau) = u^k$. The solution of the polynomial equation yields τ, from which the amplitude, A, and background, B, are calculated. The algorithm is applied to each selected pixel in succession. The program has been written in Fortran and has proved to be rapid and accurate when ~10 image time points are gathered. Details will be presented at a later date.

We thank Ellie Mann for help with the manuscript, and Dr. Marriott wishes to thank the Alexander von Humboldt Stiftung for generous fellowship support.

Received for publication 25 January 1991 and in final form 1 May 1991.

REFERENCES

Aikens, R. S., D. A. Agard, and J. W. Sedat. 1989. Solid-state imagers for microscopy. *Methods Cell Biol.* 29:291–313.

Arndt-Jovin, D. J., M. Robert-Nicoud, S. J. Kaufman, and T. M. Jovin. 1985. Fluorescence digital imaging microscopy in cell biology. *Science (Wash. DC).* 230:247–256.

Austin, R. H., S. S. Chan, and T. M. Jovin. 1979. Rotational diffusion of cell surface components by time-resolved phosphorescence. *Proc. Natl. Acad. Sci. USA.* 76:5650–5654.

Becquerel, E. 1868. *In* La Lumiere. Ses Causes et Ses Effets. Librairie de Firmin Didot Fréres, Paris. I:240–250.

Beverloo, H. B., A. van Schadewijk, S. van Gelderen-Boele, and H. J. Tanke. 1990. Inorganic phosphors as new luminescent labels for immunocytochemistry and time-resolved microscopy. *Cytometry.* 11:784–792.

Carmichael, I., and G. L. Hug. 1989. CRC Handbook of Organic Photochemistry. Vol. 1. J. C. Scaiano, editor. CRC Press, Boca Raton, FL. 369–403.

Corin, A. F., E. D. Matayoshi, and T. M. Jovin. 1985. Triplet state spectroscopy for investigating diffusion and chemical kinetics. *In* Spectroscopy and the Dynamics of Molecular Biological Systems. P. M. Bayley, R. R. Dale, editors. Academic Press, Inc., New York. 53–78.

Corin, A. F., and T. M. Jovin. 1986. Proflavin binding to poly[d(A-T)] and poly[d(A-br^{5}U)]: triplet state and temperature-jump kinetics. *Biochemistry.* 25:3995–4007.

Darzynkiewicz, Z. 1979. Acridine orange as a molecular probe in studies of nucleic acids in situ. *In* Flow Cytometry and Sorting. M. R. Melamed, P. F. Mullaney, and M. L. Mendelsohn, editors. John Wiley & Sons, New York. 285–316.

Darzynkiewicz, Z., and J. Kapuscinski. 1990. Acridine orange: a versatile probe of nucleic acids and other cell constituents. *In* Flow Cytometry and Sorting, 2nd ed. M. R. Melamed, T. Lindmo, and M. L. Mendelsohn, editors. John Wiley & Sons, New York. 291–314.

DeBiasio, R., G. R. Bright, L. A. Ernst, A. S. Waggoner, and D. L. Taylor. 1987. Five-parameter fluorescence imaging: wound healing of living Swiss 3T3 cells. *J. Cell Biol.* 105:1613–1622.

Delic, J., J. Coppey, H. Magdelenat, and M. Coppey-Moisan. 1991. Impossibility of acridine orange intercalation in nuclear DNA of the living cell. *Exp. Cell Res.* 194:147–153.

Delorme, R., and F. Perrin. 1929. Durées de fluorescence des sels duranyle solides et de leurs solutions. *J. Phys. Rad.* 10:177–186.

Englander, S. W., D. B. Calhoun, and J. J. Englander. 1987. Biochemistry without oxygen. *Anal. Biochem.* 161:300–306.

Garland, P. B., and C. H. Moore. 1979. Phosphorescence of protein-bound eosin and erythrosin. *Biochem. J.* 183:561–572.

Geacintov, N. E., J. Waldmeyer, V. A. Kuymin, and T. Kolubayev. 1981. Dynamics of the binding of acridine dyes to DNA investigated by triplet excited state probe techniques. *J. Phys. Chem.* 85:3608–3613.

Gratton, E., and D. M. Jameson. 1985. New approach to phase and modulation resolved spectra. *Anal. Chem.* 57:1694–1697.

Harvey, E. N., and A. M. Chase. 1942. The phosphorescence microscope. *Rev. Sci. Instr.* 13:365–368.

Haugland, R. P. 1989. Fluorescein substitutes for microscopy and imaging. *In* Optical Microscopy for Biology. B. Herman and K. Jacobson, editors. Wiley-Liss, New York. 143–157.

Hemillä, L., S. Dakubu, V.-M. Mukkala, H. Siitari, and T. Lövgren. 1984. Europium as a label in time-resolved immunofluorometric assays. *Anal. Biochem.* 137:335–343.

Hiraoka, Y., J. W. Sedat, and D. A. Agard. 1987. The use of a charge-coupled device for quantitative optical microscopy of biological structures. *Science (Wash. DC).* 238:36–41.

Ho, W. C., V. J. Allan, G. v. Meer, E. G. Berger, and T. E. Kreis. 1989. Reclustering of scattered Golgi elements occurs along microtubules. *Eur. J. Cell Biol.* 48:250–263.

Johnson, P., and P. B. Garland. 1981. Depolarization of fluorescence depletion. *FEBS Letts.* 132:252–256.

Jovin, T. M. and D. J. Arndt-Jovin. 1989. Luminescence digital imaging microscopy. *Annu. Rev. Biophys. Biophys. Chem.* 18:271–308.

Jovin, T. M., G. Marriott, R. M. Clegg, and D. J. Arndt-Jovin. 1989. Photophysical processes exploited in digital imaging microscopy: fluorescence resonance energy transfer and delayed luminescence. *Ber. Bunsenges. Phys. Chem.* 93:387–391.

Jovin, T. M., and W. Vaz. 1989. Rotational and translational diffusion. *Meth. Enzymol.* 172:471–513.

Jovin, T. M., D. J. Arndt-Jovin, G. Marriott, R. M. Clegg, M. Robert-Nicoud, and T. Schormann. 1990. Distance, wavelength and time: the versatile 3rd dimensions in light emission microscopy. *In* Optical Microscopy for Biology. B. Herman and K. Jacobson, editors. Wiley-Liss, New York. 575–602.

Kasten, F. H. 1989. The origins of modern fluorescence microscopy and fluorescence probes. *In* Cell Structure and Function by Microspectrofluorometry. E. Kohen and J. G. Hirschberg, editors. Academic Press, New York. 3–50.

Kautsky, H., A. Hirsch, and W. Flesch. 1935. Energie-Umwandlung an Grenzflächen, VIII Mitteil.: Die Bedeutung Metastablischer Zustände für Sensibilisierte Photo-oxidationen. *Ber. dtsch. Chem. Ges.* 68:152–162.

Kohen, E., and J. G. Hirschberg, editors. 1989. Cell Structure and Function by Microspectrofluorometry. Academic Press, New York.

Lipsky, N. G., and R. E. Pagano. 1985. A vital stain for the Golgi apparatus. *Science (Wash. DC).* 228:745–747.

O'Haver, T. C., and W. M. Parks. 1974. Selective modulation: a new instrumental approach to the fluorimetric analysis of mixtures without separation. *Anal. Chem.* 46:1886–1894.

Parker, C. A. 1968. Photoluminescence of Solutions. Elsevier, Amsterdam.

Piston, D. W., G. Marriott, T. Radivoyevich, R. M. Clegg, T. M. Jovin, and E. Gratton. 1989. Wide-band acousto-optic light modulator for frequency domain fluorometry and phosphorimetry. *Rev. Sci. Instrum.* 60:2596–2600.

Polyakov, Y. S., Y. M. Rosanov, and E. M. Brumberg. 1966. The setting installation for studying the phosphorescence of microobjects. *Cytologie SSSR.* 8:677–681.

Rigler, R. 1966. Microfluorometric characteristics of intracellular nucleic acids and nucleoproteins by acridine orange. *Acta Physiol. Scand.* 67:4–121.

Robbins, E., and P. I. Marcus. 1963. Dynamics of acridine orange-cell interaction. I. Interrelationships of acridine orange particles and cytoplasmic reddening. *J. Cell. Biol.* 18:237–250.

Robbins, E., Marcus, P. J., and N. K. Gonatas. 1964. Dynamics of acridine orange-cell interaction. II. Dye-induced ultrastructural changes in multivesicular bodies (acridine orange particles). *Cell Biol.* 19:49–64.

Rumsey, W. L., J. M. Vanderkooi, and D. F. Wilson. 1988. Imaging of phosphorescence: a novel method of measuring oxygen distribution in perfused tissue. *Science (Wash. DC).* 241:1649–1651.

Steiner, R. F., I. Weinryb, and R. Kolinski. 1970. The low temperature luminescence of complexes of acridine orange with polyelectrolytes. *Biochim. Biophys. Acta.* 209:309–319.

Taylor, D. L., and Y. L. Wang, editors. 1989. Methods Cell Biol. Academic Press, Inc., CA. Vols. 29 and 30.

Tsien, R. Y. 1989. Fluorescent indicators of ion concentrations. *Methods Cell Biol.* 30:127–156.

Vanderkooi, J. M., G. Maniara, T. J. Green, and D. F. Wilson. 1987. An optical method for measurement of dioxygen concentration based upon quenching of phosphorescence. *J. Biol. Chem.* 262:5476–5482.

Vialli, M. 1964. Indirizzi di ricerca nel campo della istoluminescenza. *Z. wiss. Mikrosk.* 66:164–170.

Zanker, V. 1952. Quantitative Absorptions-und Emissionsmessungen am Acridinorangekation. *Z. physik. Chemie.* 199:225–292.

Zelenin, A. V. 1966. Fluorescence microscopy of lysozomes and related structures in living cells. *Nature (Lond.).* 212:425–426.

Zotikov, A. A. 1982. Some possibilities of the phosphorescence microscopy for the study of cells and chromatin. *Acta Histochem.* 26 (suppl):215–217.

Zotikov, A. A., and Y. S. Polyakov. 1975. Investigation of the phosphorescence of cells of various types with the phosphorescence microscope. *Izvestiya Akademii Nauk. SSSR Seriya. Biol. Esckaya.* 2:277–280.

Zotikov, A. A., and Y. S. Polyakov. 1977. The use of the phosphorescence microscope for the study of the phosphorescence of various cells. *Microscop. Acta.* 79:415–418.